Stépán, G., Delay-differential equation models for machine tool chatter
in *Nonlinear Dynamics of Material Processing and Manufacturing*
Ed.: F. C. Moon, John Wiley & Sons, New York, 1998, 165-192.

Delay-differential equation models for machine tool chatter

GÁBOR STÉPÁN
Department of Applied Mechanics
Technical University of Budapest
Budapest H-1521, Hungary

Machine tool chatter is one of the most complex dynamical processes. Since the accuracy of a machine tool is strongly affected by the vibrations arising during the cutting process, several models appeared in the specialist literature to explain and to predict these vibrations. From dynamical systems view-point, the most complicated models are the ones which describe the so-called self-excited vibrations of the machine tools. Within this group of models, the complexity of the model increases with the number of degrees of freedom, i.e. with the dimension of the phase space where the trajectories are embedded. The greater the dimension of the phase space is, the more complex the described dynamical phenomena can be.

An essential cause of the vibrations in the cutting process is the regenerative effect. Its mechanical model can still be a single degree of freedom system, but the corresponding mathematical model is an infinite dimensional one. The presence of the time delay results delay-differential equations (DDE), and the trajectories can uniquely be described in an infinite dimensional phase space only. Since the mechanical model can still be simple and deterministic, there is a possibility for analytical, often closed form calcula-

tions and the topological description of trajectories may present complicated, even chaotic nonlinear vibrations. If we take a careful look at the experimental results, they always contain more or less stochastic components. Since the numerical simulation of the complex models may or may not include stochasticity which refers to the dynamics of the model and the discretization technique together, it is important to predict nonlinear vibrations also with analytical work now involving computer algebra, too.

First, we summarize briefly the stability analysis of linear autonomous DDEs. Some of the stability charts relevant in modelling oscillatory systems with delay are also presented. Then simple mechanical models are given for regenerative machine tool chatter. The construction of basic stability charts in the plane of the technological parameters is explained. Finally, local and global nonlinear phenomena are described when the nonlinearity occurring in the DDE model is related to the cutting force. Delay differential equations with time periodic coefficients are not discussed here. Note, however, that such mathematical models are also important in modelling machine tool vibrations in case of milling, when the number of cutting edges working together varies in time (see e.g. Minis, 1994).

1 GUIDE TO DELAY-DIFFERENTIAL EQUATIONS

The simplest DDE has the form

$$\dot{x}(t) = x(t-1) \tag{1}$$

where the state variable x is scalar, $x(t) \in \mathbb{R}$, dot stands for differentiation with respect to the time t, and the time delay is just 1. The DDE describes a system where the present rate of change of state depends on a past value of the state. Substituting the trial solution $x(t) = Ke^{\lambda t}$, $K, \lambda \in \mathbb{C}$ we obtain a non-trivial solution for K when

$$(\lambda - \mathrm{e}^{-\lambda})Ke^{\lambda t} \quad \Rightarrow \quad \lambda - \mathrm{e}^{-\lambda} = 0\,.$$

The latter equation is also called characteristic equation which has infinitely many solutions for the complex characteristic roots λ_j , $j = 1, 2, \ldots$. As this

simple example suggests, the theory of DDEs is a quite direct generalization of the theory of ordinary differential equations (ODE) into infinite dimensional phase spaces. This generalization is not a trivial task, though, and it uses the mathematical tools developed for functional differential equations (FDE). For a thorough introduction into this theory see the books (Hale 1977; Kuang, 1993).

In case of linear, time-independent mechanical models describing vibratory systems in the presence of time delay, the most general mathematical model assumes the form

$$\mathbf{M}\ddot{\mathbf{x}}(t) + \int_{-r}^{0} \mathrm{d}\mathbf{B}(\theta)\dot{\mathbf{x}}(t+\theta) + \int_{-r}^{0} \mathrm{d}\mathbf{C}(\theta)\mathbf{x}(t+\theta) = 0\,. \tag{2}$$

It has a similar structure to the well-known matrix differential equation of small oscillations in a finite degree of freedom (DOF) system about its stable equilibrium. In this equation, $\mathbf{x}(t) \in \mathbb{R}^n$ where the mechanical system has n DOF. The constant matrix $\mathbf{M}$ is the usual symmetric and positive definit mass matrix, while the matrices $\mathbf{B}, \mathbf{C}$ describe the weights of some past-effects with respect to the 'damping' and the 'stiffness' in the system back in the time till $t - r$. The elements of $\mathbf{B}(\theta) = [b_{jk}(\theta)]$, $\mathbf{C}(\theta) = [c_{jk}(\theta)]$ are functions of bounded variation, and the corresponding terms in (2) contain the so-called Stieltjes integrals. This is a kind of short-hand which is very convenient to describe two different types of delays which will also appear in regenerative machine tool chatter models. One is the 'discrete delay' τ, the other is the 'continuous delay' described by a weight function w over a certain time interval. For example, the scalar:

$$c(\theta) = \begin{cases} 0 & \theta \in [-r, -\tau) \\ -1 & \theta \in [-\tau, -h) \\ h - 1 + \theta + \frac{h}{\pi}\sin(\theta\pi/h) & \theta \in [-h, 0) \\ h & \theta = 0 \end{cases} \tag{3}$$

in Figure 1 gives

$$\int_{-r}^{0} x(t+\theta)\mathrm{d}c(\theta) = x(t) + \int_{-h}^{0} (1 + \cos(\theta\pi/h))x(t+\theta)\mathrm{d}\theta - x(t-\tau)\,,$$

since $\mathrm{d}c(\theta) = \dot{c}(\theta)\mathrm{d}\theta$ where c is differentiable, and $\mathrm{d}c(\theta) = c(\theta+0) - c(\theta-0)$ where c has a discontinuity. Thus, the coefficients of the discrete delay terms

at 0 and $-\tau$ are

$$c(+0) - c(-0) = +1 \quad \text{and} \quad c(-\tau + 0) - c(-\tau - 0) = -1$$

while the weight function for the continuous time delay term is

$$w(\theta) = \frac{\mathrm{d}}{\mathrm{d}\theta} c(\theta) = 1 + \cos(\theta\pi/h)\,, \quad \theta \in [-h, 0)\,.$$

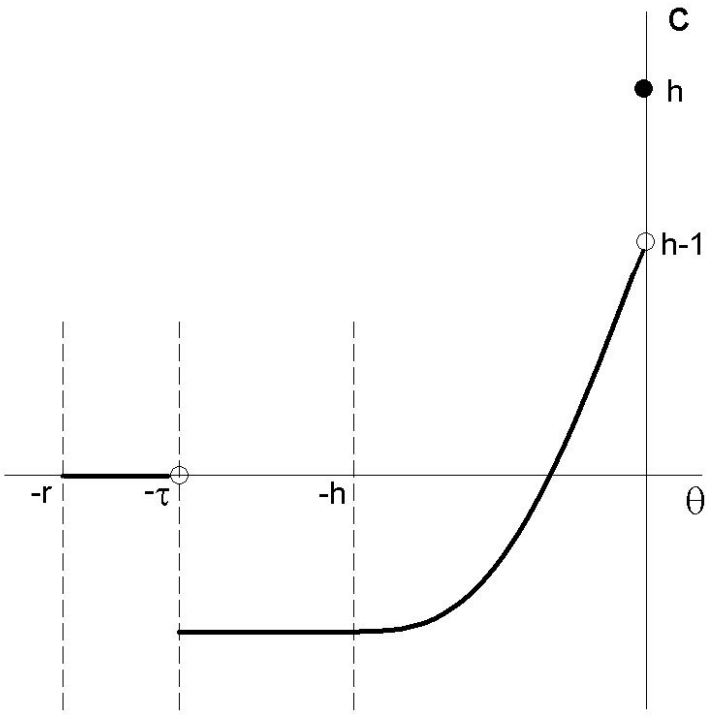

Figure 1: Description of discrete and continuous delays with (3)

The trivial solution $\mathbf{x} \equiv \mathbf{0}$ of the DDE (2) is not necessarily stable, of course. However, the necessary and sufficient condition for asymptotic stability is the same as it is for ODEs: the real parts of all the (infinitely many) characteristic roots have negative real parts. These characteristic roots are the zeros of the transcendental characteristic function

$$D(\lambda) = \det\left(\mathbf{M}\lambda^2 + \int_{-r}^{0} \lambda \mathrm{e}^{\lambda\theta} \mathrm{d}\mathbf{B}(\theta) + \int_{-r}^{0} \mathrm{e}^{\lambda\theta} \mathrm{d}\mathbf{C}(\theta)\right) \tag{4}$$

obtained by substituting the trial solution $\mathbf{K}e^{\lambda t}$ into the DDE (2) as shown in the introductory scalar example (1).

The infinite dimensional version of the Routh-Hurwitz criterion used for the characteristic polynomial of ODEs is needed to analyze the zeros of the characteristic functions (4) of DDEs. If we define the real functions

$$R(\omega) = \mathrm{Re}\, D(\mathrm{i}\omega)\,, \quad S(\omega) = \mathrm{Im}\, D(\mathrm{i}\omega)\,, \quad \omega \in [0, \infty)\,, \tag{5}$$

and the real zeros of R are denoted by $\rho_1 \geq \ldots \rho_r \geq 0$, i.e.

$$R(\rho_k) = 0\,, \quad k = 1, \ldots, r$$

then the equilibrium of the linear delayed mechanical system (2) of n DOF is asymptotically stable if and only if

$$S(\rho_k) \neq 0\,,\ k = 1, \ldots, r \quad \text{and} \tag{6}$$

$$\sum_{k=1}^{r} (-1)^k \mathrm{sgn}\, S(\rho_k) = (-1)^n n\,. \tag{7}$$

In case of n DOF systems, the dimension of the phase space is $2n$, i.e. always even. The above mentioned stability criterion has a somewhat more complicated form for DDEs with odd dimensions (like (1) — see further details in Stépán 1989).

In the following section, the most important stability charts are summarized for delayed vibratory systems. These are presented and explained for simple cases having the minimum number of mathematical parameters only, and later these charts will be referred to when the equations of regenerative machine tool chatter are analyzed fully loaded with the necessary mechanical and technological parameters and parameter functions.

2 BASIC STABILITY CHARTS OF DELAYED VIBRATORY SYSTEMS

A stability chart presents those domains in the space of the system parameters where the equilibrium is asymptotically stable. By presenting the number of the pure imaginary (or zero) characteristic roots along the stability limits it can also refer to the way the equilibrium loses its stability.

The stability limits can be determined in the parameter space (often plane) by plotting the co-dimension 1 surfaces (often curves) given by the so-called D-curves:

$$R(\omega) = 0\,, \quad S(\omega) = 0\,, \quad \omega \in [0, \infty) \tag{8}$$

where R, S are defined in (5) by means of the characteristic function D, and ω takes the role of the parameter of the curve. In general, these curves separate infinitely many disjunct domains, and we need the stability criteria (6,7) to select the ones which correspond to asymptotic stability.

As an introductory example consider the simple first order scalar DDE

$$\dot{x}(t) + c \int_{-\infty}^{0} w(\theta) x(t+\theta) \mathrm{d}\theta = 0\,, \quad b \in \mathbb{R}\,. \tag{9}$$

The weight function

$$w(\theta) = \mathrm{e}^{\theta/\tau}\,, \quad \theta \in (-\infty, 0] \tag{10}$$

is often used to model delay effects with a simple approximation. The effect of the past is fading away exponentially in the past, and $\tau > 0$ is assumed as a measure of the delay in the system. The characteristic function

$$D(\lambda) = \lambda + c \int_{-\infty}^{0} \mathrm{e}^{\theta/\tau} \mathrm{e}^{\theta\lambda} \mathrm{d}\theta = \lambda + c \frac{1}{\lambda + 1/\tau}$$

has two zeros only which also come from the polinomial

$$\lambda^2 + \lambda/\tau + c\,. \tag{11}$$

The Routh-Hurwitz criterion implies that the trivial solution of (9) is asymptotically stable if and only if $c > 0$. The analysis of this DDE is easy since the delay with this exponential weight function increases the dimension of the system by one only. It can be shown that the DDE (9) with the weight function (10) is equivalent to a second order ODE. Differentiate (9) with respect to the time t, and use partial integration to calculate

$$\begin{aligned} &\ddot{x}(t) + c \int_{-\infty}^{0} \mathrm{e}^{\theta/\tau} \dot{x}(t+\theta) \mathrm{d}\theta = \\ &\ddot{x}(t) + cx(t) - \frac{c}{\tau} \int_{-\infty}^{0} \mathrm{e}^{\theta/\tau} x(t+\theta) \mathrm{d}\theta = \\ &\ddot{x}(t) + \frac{1}{\tau} \dot{x}(t) + cx(t)\,. \end{aligned} \tag{12}$$

Its characteristic polinomial is just (11).

In case of oscillatory mechanical systems without viscous damping, the D-curves are usually lines in the parameter plane. The examples with finite and continuous delay like

$$\ddot{x}(t) + c_0 x(t) - c_1 \int_{-1}^{0} w(\theta) x(t+\theta) \mathrm{d}\theta = 0 \tag{13}$$

with the simplest weight function

$$w(\theta) \equiv 1\,, \quad \theta \in [-1, 0] \tag{14}$$

have the characteristic function

$$D(\lambda) = \lambda^2 + c_0 - c_1 \int_{-1}^{0} \mathrm{e}^{\lambda\theta} \mathrm{d}\theta = \lambda^2 + c_0 - c_1 \frac{1 - \mathrm{e}^{-\lambda}}{\lambda}\,, \ \lambda \neq 0 \tag{15}$$

with understanding

$$D(0) = \lim_{\lambda \to 0} D(\lambda) = c_0 - c_1\,,$$

of course. Since the D-curves (8) have the form

$$R(\omega) = -\omega^2 + c_0 - c_1 \frac{\sin\omega}{\omega} = 0\,, \quad S(\omega) = c_1 \frac{1 - \cos\omega}{\omega} = 0\,,$$

the zeros of S can be given as $\omega = 2k\pi\,,\ k = 0, 1, \ldots$ or $c_1 = 0$, and the D-curves in the plane of c_0, c_1 are lines, indeed

$$c_1 = 0 \text{ and } c_0 > 0\,, \quad c_1 = c_0\,, \quad c_0 = 4k^2\pi^2\,.$$

The criteria (6),(7) with $n = 1$ DOF can be used to select the stability regions bordered by these lines. The first condition (6) clearly gives

$$c_0 \neq 4k^2\pi^2 \quad k = 1, 2, \ldots\,. \tag{16}$$

If

$$0 < c_1 < c_0 \tag{17}$$

then

$$R(0) = c_0 - c_1 > 0 \quad \text{and} \quad \lim_{\omega \to \infty} R(\omega) = -\infty\,, \tag{18}$$

and the number r of the real positive zeros of R is odd, while S is positive at all the zeros ρ_k of R due to (16), so

$$\sum_{k=1}^{r}(-1)^k \mathrm{sgn}\, S(\rho_k) = \sum_{k=1}^{r}(-1)^k = -1$$

and the stability condition (7) is satisfied. If either $c_1 < 0$ or $c_1 > c_0$ then this condition is not satisfied. The stability chart of Figure 2 shows the shaded stability domains determined by the necessary and sufficient conditions (16,17) for asymptotic stability. This example calls the attention for the difficulty of selecting stability domains just by drawing the D-curves. Although the criteria (60,(7) will not be checked and analyzed in the subsequent examples, we emphasize their importance in the construction of the stability charts.

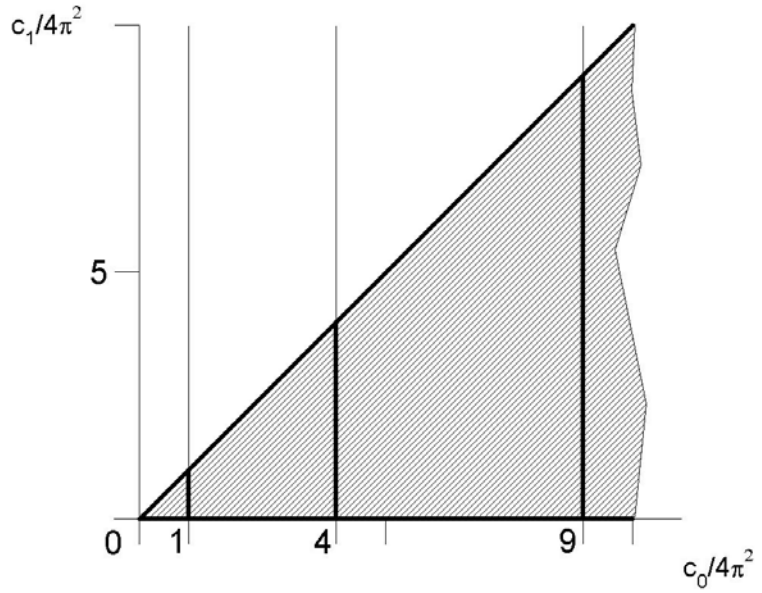

Figure 2: Stability chart of DDE (13) with (14)

If the DDE (13) is considered with the weight function

$$w(\theta) = -\frac{\pi}{2}\sin(\pi\theta)\,, \quad \theta \in [-1, 0] \tag{19}$$

then the characteristic function reads

$$D(\lambda) = \lambda^2 + c_0 - c_1 \frac{\pi^2}{2} \frac{1 + \mathrm{e}^{-\lambda}}{\lambda^2 + \pi^2}\,, \ \lambda \neq \pm \mathrm{i}\pi$$

with a continuous extension at $\pm\mathrm{i}\pi$, i.e. with

$$D(\pm\mathrm{i}\pi) = \lim_{\lambda \to \pm\mathrm{i}\pi} D(\lambda) = -\pi^2 + c_0 \pm \mathrm{i}\frac{\pi}{4} c_1\,.$$

This results the D-curves

$$R(\omega) = -\omega^2 + c_0 - c_1 \frac{\pi^2}{2} \frac{1 + \cos\omega}{\pi^2 - \omega^2} = 0\,, \quad S(\omega) = c_1 \frac{\pi^2}{2} \frac{\sin\omega}{\pi^2 - \omega^2} = 0$$

where $S = 0$ can be solved in closed form again giving $c_1 = 0$ or $\omega = j\pi,\ j = 0, 2, 3, \ldots$ (note $j \neq 1$). Substituting these into $R = 0$ we obtain the following lines as D-curves:

$$c_1 = 0 \text{ and } c_0 > 0\,, \quad c_1 = c_0\,, \quad \frac{1 + (-1)^j}{2} c_1 = -(j^2 - 1)(c_0 - j^2\pi^2)\,,\ j = 2, 3, \ldots$$

In the corresponding stability chart of Figure 3 the shaded stability regions selected by (6,7) are bordered by these lines. The ω values above the stability chart represent the critical angular frequencies at the corresponding stability limits.

The comparison of the stability charts in Figures 2 and 3 for the same DDE shows the great influence of the shape of the weight function on stability, both weight functions satisfy

$$\int_{-1}^{0} w(\theta)\mathrm{d}\theta = 1\,, \quad \int_{-1}^{0} \theta w(\theta)\mathrm{d}\theta = -\frac{1}{2}\,,$$

though.

The DDE

$$\ddot{x}(t) + b_0\dot{x}(t) + c_0 x(t) - c_1 x(t-1) = 0 \tag{20}$$

can also be assumed as a special case of the DDE (13) when $b_0 = 0$, i.e. there is no damping in the system, and the weight function is the so-called Dirac function at -1, i.e. $w(\theta) = \delta(1 + \theta)$. The D-curves calculated from the characteristic function

$$D(\lambda) = \lambda^2 + b_0\lambda + c_0 - c_1\mathrm{e}^{-\lambda} \tag{21}$$

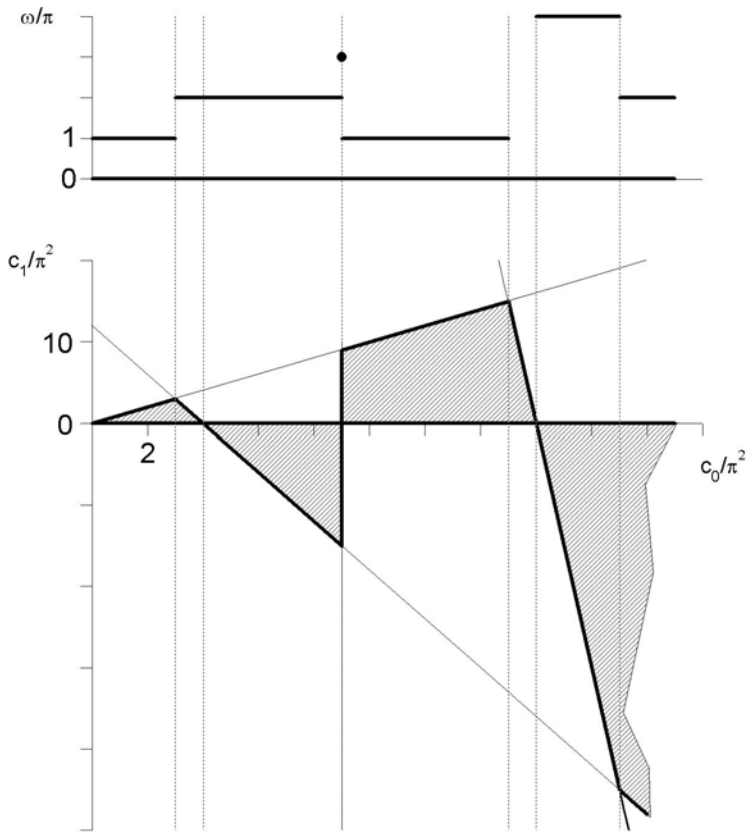

Figure 3: Stability chart of DDE (13) with (19)

can be given as:

$$R(\omega) = -\omega^2 + c_0 - c_1 \cos\omega = 0\,, \quad S(\omega) = b_0\omega + c_1 \sin\omega = 0\,.$$

When $b_0 = 0$, these are equivalent to

$$c_1 = 0 \text{ and } c_0 > 0\,, \quad (-1)^j c_1 = c_0 - j^2\pi^2\,,\ j = 0, 1, \dots\,,$$

which border the shaded stability regions in Figure 4 presenting a similar structure to that of Figure 3. Figure 5 also shows the stability regions when $b_0 = 1$. The damping increases the regions of stability, but the D-curves are not straight lines any more:

$$c_0 = \omega^2 - \frac{\omega}{\tan\omega}\,, \quad c_1 = -\frac{\omega}{\sin\omega}\,, \quad \omega \neq 0, \pi, 2\pi, \dots$$

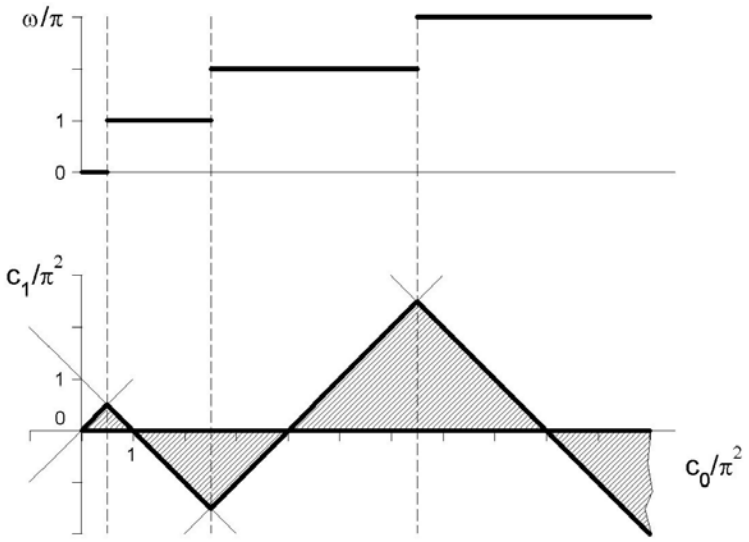

Figure 4: Stability charts of DDE (20) with $b_0 = 0$

Finally, the stability chart of the DDE

$$\frac{\mathrm{d}^3}{\mathrm{d}t^3}x(t) + b_0\frac{\mathrm{d}}{\mathrm{d}t}x(t) - c_1x(t-1) = 0 \tag{22}$$

is presented in Figure 6. The structure of this chart is the same again with the important difference that the stability domains are located in the half-plane $c_1 < 0$ only. This kind of DDE of odd order becomes important when continuous delay with an exponential weight function (10) is added to an oscillatory system already having a discrete delay.

The stability chart also serves information about possible non-linear vibrations in that non-linear system the linearization of which is the corresponding linear DDE. All the stability limits but the ones $c_1 = c_0$ in the stability charts of Figures 3, 4, 5 and $c_1 = 0$ in Figure 6 refer to possible Hopf bifurcations with critical characteristic roots $\pm\mathrm{i}\omega$ presented above the charts. Stable or unstable periodic motions may appear there with angular frequency at about ω.

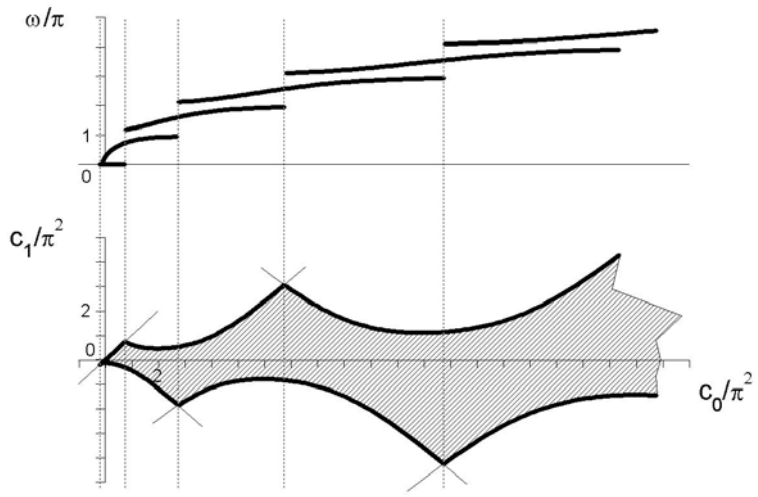

Figure 5: Stability charts of DDE (20) with $b_0 = 1$

3 BASIC DDE MODELS OF REGENERATIVE MACHINE TOOL CHATTER

The basic idea of the regenerative effect is well understood in the specialist literature (Tlusty and Spacek 1954; Tobias 1965) and experiments clearly confirmed its existence. The machine tool is an elastic structure, so the tool and the workpiece can move relative to each other. In case of stationary cutting conditions, the chip thickness f, the chip width, and the cutting speed v are constant values as prescribed by the designed technology. Because of some external or internal perturbation, the single tool and the workpiece start a damped vibration relative to each other, and the surface of the workpiece becomes wavy. After a round of the workpiece (or the tool), the chip thickness will vary at the tool because of this wavy surface. Consequently, the cutting force will also vary and excite the structure. Moreover, this excitation frequency seems to be very dangerous since it is almost the same as the natural frequency of the structure. However, this phenomenon cannot be modeled as an excited vibration, it is rather a self-excited one, where the cutting force is determined by the designed technological parameters, but its variation depends on the difference of the relative displacement of the tool

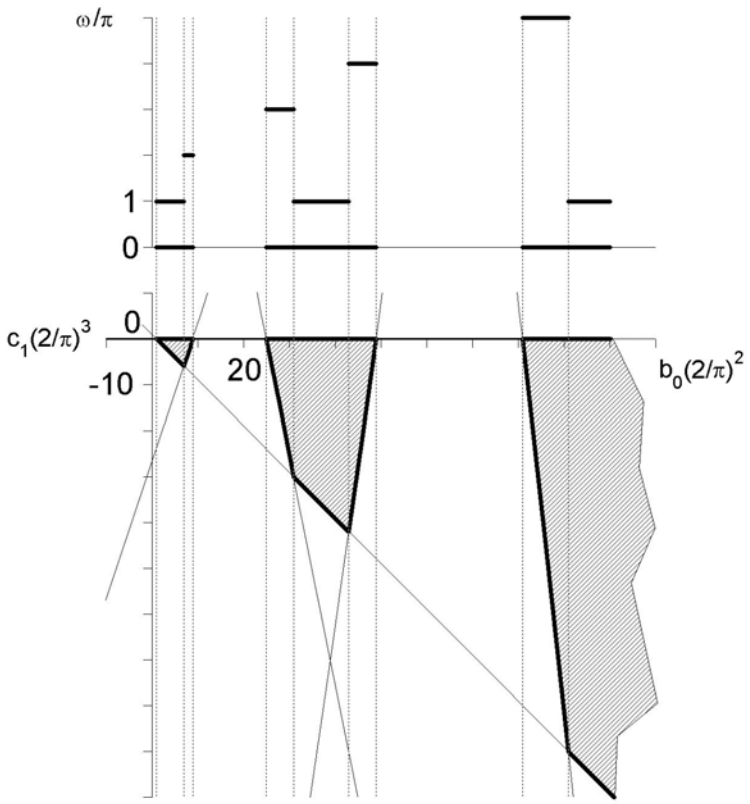

Figure 6: Stability chart of DDE (22)

and the workpiece at the given time instant and one round of the workpiece earlier. This special kind of self-excited vibration, where past effects also take place, is called regenerative vibration. In this sense, the appearance of the regenerative vibration is a stability problem in a delayed oscillatory system, in other words, in a damped oscillatory system with a delayed feed-back, or dead time.

Figure 7 shows the simplest, 1DOF mechanical model of the regenerative machine tool vibration in the planar case of the so-called orthogonal cutting. This model will allow us to explain the basic stability problems and nonlinear vibrations arising in this system. In case of industrial applications, the 1 DOF mechanical model is to be subsituted by the result of a thorough experimental modal analysis of the machine tool structure as often presented

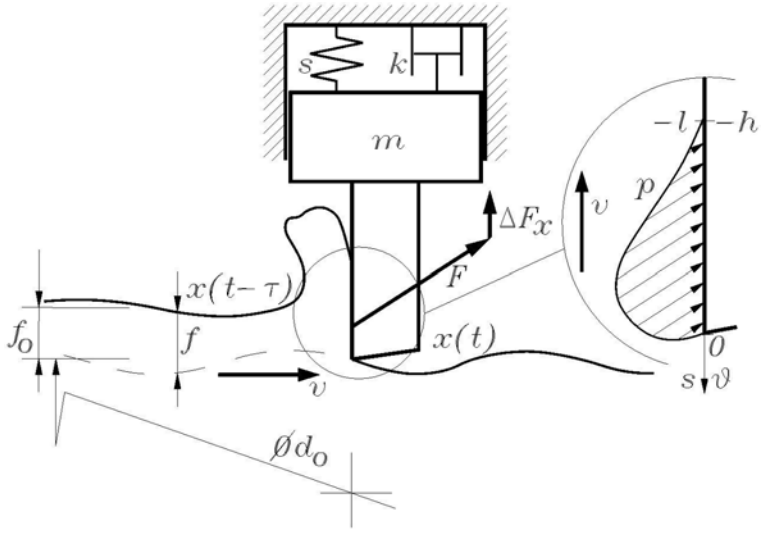

Figure 7: Mechanical model and cutting force variation

in the specialist literature (see for examle Shi and Tobias 1984). However, it is also true that the lowest natural frequencies are the most involved ones in the regenerative vibrations, and low DOF mechanical models can still serve good quantitative results.

The zero value of the coordinate x of the tool edge position is set in a way that the x component F_x of the cutting force F is in balance with the spring force while the chip thickness f is just the prescribed value f_0. Then the equation of motion of the tool is clearly

$$\ddot{x} + 2\kappa\alpha\dot{x} + \alpha^2 x = \frac{1}{m}\Delta F_x(f) \tag{23}$$

where $\alpha = \sqrt{c/m}$ is the natural angular frequency of the undamped free oscillating system, and $\kappa = b/(2m\alpha)$ is the so-called relative damping factor. The calculation of the cutting force variation ΔF_x requires an expression of the cutting force as a function of the technological parameters, primarly as a function of the chip thickness f which depends on the position x of the tool edge.

A simple but empirical way to calculate the cutting force is the application of the so-called Taylor formulae. According to this, the cutting force F_x^T

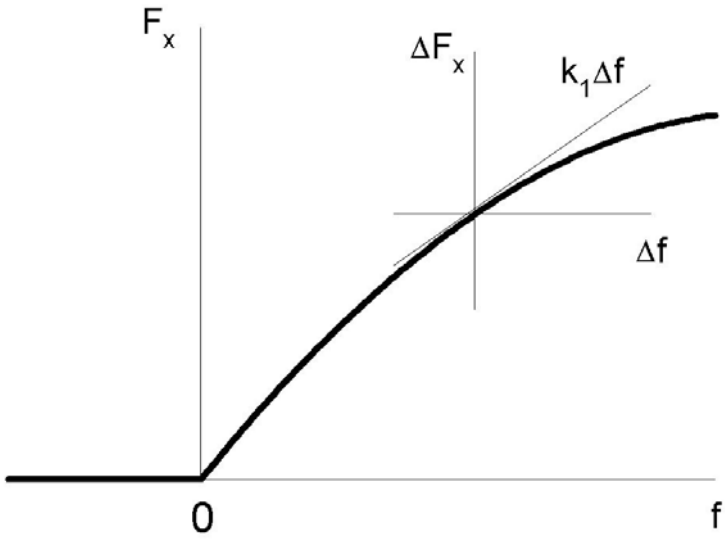

Figure 8: Cutting force and chip thickness relation

depends on the chip thickness as shown in Figure 8 where the superscript T refers to the Taylor approximation. This is a degressive function usually given as a certain power of f which is less than 1. This might be convenient in some technological design algorithms, but dynamical calculations prefer a power series form around f_0 like

$$\Delta F_x^T(f) = F_x^T(f) - F_x^T(f_0) = \begin{cases} \sum_{j=1}^{p} k_j (\Delta f)^j & \text{if } \Delta f > -f_0 \\ -F_x^T(f_0) & \text{if } \Delta f \leq -f_0 \end{cases} \tag{24}$$

where the chip thickness variation is

$$\Delta f = f - f_0\,, \tag{25}$$

the so-called *cutting force coefficient*

$$k_1 = \frac{\mathrm{d}F_x^T(f_0)}{\mathrm{d}f} \tag{26}$$

describes the linear approximation of the cutting force variation, and the further coefficients of the power series come from

$$k_j = \frac{\mathrm{d}^j F_x^T(f_0)}{j!\mathrm{d}f^j}\,, \quad j = 2, 3, \ldots\,. \tag{27}$$

Note that the cutting force is zero for negative chip thickness ($f < 0 \Leftrightarrow \Delta f < -f_0$), which does not exist physically, of course. This is an important non-linear part of the cutting force variation to be discussed later.

An improved way to calculate the cutting force is to determine the stress resultant of the distributed force system P along the active face of the tool:

$$F_x(f) = \int_{-l}^{0} P_x(f, s)\mathrm{d}s\,. \tag{28}$$

This is a challenging task of continuum mechanics. Although some early results can be found in the literature (Usui, Shirakashi and Kitagawa 1978), the most precise and detailed results has been published recently (Marusich and Ortiz 1996). Their finite element algorithm accounts for inertia effects, contact and friction, heat generation and conduction, thermal softening, mechanical hardening, rate-sensitivity, brittle and ductile fracture and fragmantation, and permits chip morphologies as a function of the technological parameters. This finite element calculation can trace the rigid body dynamics, too, but the great amount of numerical work does not allow us to have analytical study of the regenerative effect and to produce stability charts to summarize the effect of system and technological parameters on stability. As shown later, however, the variation of the distributed force system P on the active face of the tool has an important role in the dynamics of the system. The following approximation of the x component P_x of the force system combines the Taylor approximation of the cutting force F_x^T with an estimated shape function W (with unit [1/m]):

$$P_x(f, s) = F_x^T(f)W(s)\,, \quad s \in [-l, 0]$$

where the origin of the local coordinate s is fixed to the tip of the tool and describes the distance (arc length) back along the active face having a length l, and

$$\int_{-l}^{0} W(s)\mathrm{d}s = 1\,.$$

The estimation of W may be supported by the finite element calculations mentioned above. Under stationary cutting conditions $f \equiv f_0$ and

$$F_x(f_0) = \int_{-l}^{0} P_x(f_0, s)\mathrm{d}s = F_x^T(f_0)\int_{-l}^{0} W(s)\mathrm{d}s = F_x^T(f_0)\,, \tag{29}$$

i.e. the improved calculation of the cutting force results the conventional Taylor description.

Let a long discrete time delay τ, and a short continuous one h be introduced by

$$\tau = \frac{d_0\pi}{v}\,, \quad h = \frac{l}{v}\,. \tag{30}$$

A certain point on the surface of the workpiece needs the time τ to meet the tool again, i.e. to travel one round with the cutting speed v along the circumference $d_0\pi$ of the cylindrical workpiece of diameter d_0. The speed of the chip along the active face is proportional to the cutting speed v. For the sake of simplicity, let it also be v which means that a certain particle of the chip needs the time h to slip along the active face.

The shape of the stress distribution can also be given in the time domain by introducing a 'local time' $\theta = s/v$. This 'local time' $\theta \in [-h, 0]$ is negative and gives how much earlier a certain paricle of the chip was at the tip of the tool. The stress distribution function in this 'local time' is denoted by w (with unit [1/s]):

$$w(\theta) = vW(v\theta) \quad \Rightarrow \quad \int_{-h}^{0} w(\theta)\mathrm{d}\theta = 1\,. \tag{31}$$

Express the cutting force distribution in x direction in the time domain using the global time t and the local one θ:

$$p_x(t,\theta) = P_x(f(t,\theta), v\theta) = F_x^T(f(t,\theta))\frac{1}{v}w(\theta)\,, \quad t \in [t_0,\infty)\,,\ \theta \in [-h, 0]\,. \tag{32}$$

Above the active face of the tool, the chip thickness is approximated in the time domain by

$$f(t,\theta) = f_0 + x(t-\tau+\theta) - x(t+\theta)\,, \quad t \in [t_0,\infty)\,,\ \theta \in [-h, 0]\,, \tag{33}$$

that is the chip thickness at the tool tip is assumed to be

$$f(t,0) = f_0 + x(t-\tau) - x(t)\,.$$

As a result of the above relations (28),(29),(32),(31), the power series (24) and also the chip thickness variation coming from (33), the cutting

force variation in x direction reads

$$\Delta F_x(f(t,\,.\,)) = F_x(f(t,\,.\,)) - F_x(f_0) = \int_{-l}^{0} P_x(f(t, s/v), s)\mathrm{d}s - F_x^T(f_0) =$$

$$\int_{-h}^{0} p_x(f(t,\theta),\theta) v \mathrm{d}\theta - F_x^T(f_0) = \int_{-h}^{0} (F_x^T(f(t,\theta)) - F_x^T(f_0)) w(\theta)\mathrm{d}\theta =$$

$$\int_{-h}^{0} \left\{ \begin{array}{ll} \sum_{j=1}^{p} \frac{\mathrm{d}^j F_x^T(f_0)}{j!\mathrm{d}f^j}(\Delta f(t,\theta))^j & \text{if } \Delta f(t,\theta) > -f_0 \\ -F_x^T(f_0) & \text{if } \Delta f(t,\theta) \le -f_0 \end{array} \right\} w(\theta)\mathrm{d}\theta = \tag{34}$$

$$\int_{-h}^{0} \left\{ \begin{array}{ll} \sum_{j=1}^{p} k_j (x(t-\tau+\theta) - x(t+\theta))^j & \text{if } x(t+\theta) < f_0 + x(t-\tau+\theta) \\ -F_x^T(f_0) & \text{if } x(t+\theta) \ge f_0 + x(t-\tau+\theta) \end{array} \right\} w(\theta)\mathrm{d}\theta \approx$$

$$\int_{-h}^{0} k_1 (x(t-\tau+\theta) - x(t+\theta)) w(\theta)\mathrm{d}\theta\,. \tag{35}$$

The substitution of the linearized cutting force variation (35) in the equation of motion (23) results in a linear DDE like (2) in a scalar case with weights similar to (3) with respect to the past. Its stability analysis is presented in the next section. We obtain a nonlinear DDE suitable for Hopf bifurcation calculations if the Taylor series (24) truncated at the 3rd degree ($p = 3$) is substituted in the calculation of the cutting force variation at (34). However, the global non-linear behavior is also strongly determined by that part of the non-linearity where the cutting force variation is constant, when the tool edge leaves the workpiece and the regenerative effect, i.e. the delay disappears from the system for a certain time period. The last section will deal with these non-linear effects.

4 STABILITY OF CUTTING UNDER REGENERATIVE CONDITIONS

Even the linear model of regenerative machine tool vibrations exist in several more or less modified versions in the sepcialist literature. These modifications and improvements are needed to push the theoretical results closer to the experimental observations. Some of these will be mentioned during the stability analysis of the model derived in the previous section.

Substitute the linear cutting force variation (35) into the differential equation (23) of the 1 DOF model:

$$\ddot{x}(t) + 2\kappa\alpha\dot{x}(t) + \alpha^2 x(t) +$$

$$\frac{k_1}{m}\int_{-h}^{0} w(\theta)x(t+\theta)\mathrm{d}\theta - \frac{k_1}{m}\int_{-\tau-h}^{-\tau} w(\tau+\theta)x(t+\theta)\mathrm{d}\theta = 0\,. \qquad (36)$$

The ratio of the short time delay h and the long one τ is constant:

$$q = \frac{h}{\tau} = \frac{l}{d_0\pi}$$

as it comes from their definitions in (30). From now on, the long time delay τ will be kept as a parameter, i.e.

$$h = q\tau$$

is substituted, where τ is inversely proportional to the cutting speed v or to the angular velocity Ω of the workpiece:

$$\Omega = \frac{2\pi}{\tau}\,. \qquad (37)$$

It has a unit [rad/s], of course, but in the stability charts below it is converted to [r.p.m.].

The trivial solution of (36) refers to the stationary cutting. When its stability is investigated, the D-curves coming from the characteristic function

$$D(\lambda) = \lambda^2 + 2\kappa\alpha\lambda + \alpha^2 + \frac{k_1}{m}D_0(\tau\lambda)\,, \qquad (38)$$

$$D_0(\tau\lambda) = \int_{-q\tau}^{0} w(\theta)\mathrm{e}^{\lambda\theta}\mathrm{d}\theta - \int_{-(1+q)\tau}^{-\tau} w(\tau+\theta)\mathrm{e}^{\lambda\theta}\mathrm{d}\theta \qquad (39)$$

should be calculated as defined in (5):

$$R(\omega) = -\omega^2 + \alpha^2 + \frac{k_1}{m}R_0(\tau\omega) = 0\,, \qquad (40)$$

$$R_0(\tau\omega) = \int_{-q\tau}^{0} w(\theta)\cos(\omega\theta)\mathrm{d}\theta - \int_{-(1+q)\tau}^{-\tau} w(\tau+\theta)\cos(\omega\theta)\mathrm{d}\theta\,, \qquad (41)$$

$$S(\omega) = 2\kappa\alpha\omega + \frac{k_1}{m}S_0(\tau\omega) = 0\,, \qquad (42)$$

$$S_0(\tau\omega) = \int_{-q\tau}^{0} w(\theta)\sin(\omega\theta)\mathrm{d}\theta - \int_{-(1+q)\tau}^{-\tau} w(\tau+\theta)\sin(\omega\theta)\mathrm{d}\theta\,. \qquad (43)$$

In these equations of the D-curves, all the transcendental expressions are separated in the formulae of R_0 and S_0. They depend only on the product of the time delay τ and the critical frequency ω (which also serves as a parameter for the D-curves).

The stability charts are traditionally constructed in the plane of the cutting force coefficient k_1 and the angular velocity Ω of the workpiece (see (37)), since these parameters are proportional to the width of cut and the cutting speed, respectively, so the stability chart helps technology design in a somewhat direct way. The angular frequency ω of the vibration occurring at the loss of stability is also presented above the stability chart against the running speed Ω. The D-curves (40),(42) can be rearranged with respect to these technological parameters, and the stability limits can be plotted in the (Ω, k_1) plane with the following explicit expressions where the new parameter $\psi(=\tau\omega) \in \mathbb{R}^+$ is introduced:

$$\omega(\psi) = \alpha \left(-\kappa \frac{R_0(\psi)}{S_0(\psi)} + \sqrt{1 + \kappa^2 \frac{R_0^2(\psi)}{S_0^2(\psi)}} \right) , \tag{44}$$

$$\Omega(\psi) = \frac{2\pi\omega(\psi)}{\psi} , \tag{45}$$

$$k_1(\psi) = -2\kappa\alpha m \frac{\omega(\psi)}{S_0(\psi)} , \tag{46}$$

where R_0 and S_0 are defined in (41) and (43).

Four basic cases will be considered and discussed here. The first case is when the contact length l of the chip and tool is negligiable relative to the circumference $d_0\pi$ of the workpiece. This can be modelled by choosing the Dirac function as the weight function:

$$w(\theta) = \delta(\theta) . \tag{47}$$

Then the equation (23) of motion will contain the long discrete delay τ only:

$$\ddot{x}(t) + 2\kappa\alpha\dot{x}(t) + \alpha^2 x(t) + \frac{k_1}{m}(x(t) - x(t-\tau)) = 0 ,$$

and the expressions (41) and (43) simply give

$$R_0(\tau\omega) = 1 - \cos(\tau\omega) ,$$
$$S_0(\tau\omega) = \sin(\tau\omega) .$$

Since

$$\frac{R_0(\psi)}{S_0(\psi)} = \frac{1 - \cos\psi}{\sin\psi} = \tan\frac{\psi}{2} ,$$

the parameter ψ can be eliminated from (44), and the stability limits (45) and (46) can be expressed in a more explicite form as a function of ω as follows:

$$\Omega(\omega) = \frac{\pi\omega}{j\pi - \operatorname{atn}\frac{\omega^2-\alpha^2}{2\kappa\alpha\omega}}, \quad j = 1, 2, \dots, \tag{48}$$

$$k_1(\omega) = \frac{m}{2}\frac{(\omega^2-\alpha^2)^2 + 4\kappa^2\alpha^2\omega^2}{\omega^2-\alpha^2}. \tag{49}$$

Since $k_1 > 0$, the stability limit (49) already shows that the vibrations arising at the loss of stability will have vibration frequencies somewhat greater than the natural frequency of the system, that is $\omega > \alpha$. The stability chart in Figure 9 is constructed by means of the above D-curves in the same way as shown in the basic example (20) in Figure 5. The fixed parameters are $m = 50\,[\mathrm{kg}]$, $\kappa = 0.05$, $\alpha = 775\,[\mathrm{rad/s}]$.

It is important to observe that there exist a constant lower boundary of the stability limits which can easily be calculated from (49) as its minimum where

$$\frac{\mathrm{d}k_1}{\mathrm{d}\omega}(\omega^*) = 0 \quad \Rightarrow \quad \omega^* = \alpha\sqrt{1+2\kappa}, \quad k_{1,\min} = k_1(\omega^*) = 2m\alpha^2\kappa(1+\kappa).$$

This basic stability chart is well-known from the early books on machine tool vibration (Tobias 1965). However, this stability chart has only been verified experimentally in the middle range of the cutting speed. The real cutting process shows somewhat better stability properties at low and high cutting speed. In order to explain this experimental observation, Tobias introduced the so-called dynamic cutting theory, where he inserted an additional damping in the equation of motion which was inversely proportional to the cutting speed. This effect is very slight for turning, somewhat greater in the case of milling, and the strongest for drilling. The quantitative identification of this kind of additional damping is difficult, and does not provide a universal method for the correct prediction of regenerative vibrations at low and high speed. The introduction of the idea of a complex cutting force coefficient may also help to get better quantitative agreement between theory and experiments (Tlusty 1978), but the experimental identificaiton of this cutting force coefficient as a function of cutting speed, frequency, rake angle, etc. is difficult and the results still are not reliable for any kind of cutting.

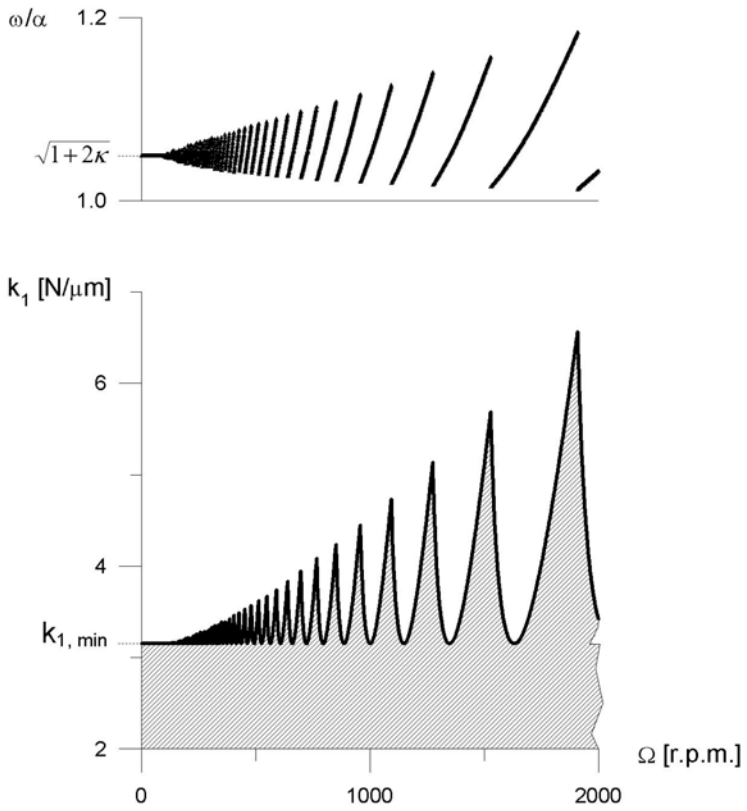

Figure 9: Stability chart with stress distribution (47)

When further weight functions W are considered in this section, we call the attention on the 'damping effect' caused by the distributed force system P acting on the tool active face. This becomes stronger as the tool-chip contact length l becomes gretaer and greater relative to the distance $d_0\pi$ between two cutting edges, i.e. as q increases. This is the smallest for turning and the greatest for drilling.

In the second case what we discuss here, the shape of the distributed cutting force system is approximated by an exponential function

$$W(s) = \frac{1}{l_0}\exp\frac{s}{l_0} \quad \Rightarrow \quad w(\theta) = \frac{v}{l_0}\exp\left(\frac{v}{l_0}\theta\right) = \frac{1}{q_0\tau}\exp\frac{\theta}{q_0\tau}\,,\ \theta \in (-\infty, 0] \tag{50}$$

where the contact length is infinite, but still, the length of this short delay

effect can be characterized by l_0, or by the ratio

$$q_0 = \frac{l_0/v}{d_0\pi/v} = \frac{h_0}{\tau}\,.$$

In the same way as in the basic example (9) and the equivalent equation (12), the equation of motion (36) can be transformed into a higher (here third) order system without a continuous time delay, but still having the discrete delay τ:

$$q_0\tau\frac{\mathrm{d}^3x}{\mathrm{d}t^3}(t) + (1+2\kappa\alpha q_0\tau)\frac{\mathrm{d}^2x}{\mathrm{d}t^2}(t) + \\ (2\kappa\alpha+\alpha^2 q_0\tau)\frac{\mathrm{d}x}{\mathrm{d}t}(t) + (\alpha^2+\frac{k_1}{m})x(t) - \frac{k_1}{m}x(t-\tau) = 0\,.$$

The stability of this kind of equation can be analyzed in the same way as shown in Figure 6 for (22), but the stability limits will not be straight lines, of course. The D-curves are constructed from (45) and (46) with

$$R_0(\psi) = \frac{1-\cos\psi+q_0\psi\sin\psi}{1+q_0^2\psi^2}\,, \quad S_0(\psi) = \frac{\sin\psi-q_0\psi(1-\cos\psi)}{1+q_0^2\psi^2}$$

calculated by partial integration from the formuale (41) and (43). The results are summarized in the stability chart of Figure 10 where the damping effect at low cutting speed appears clearly showing a good qualitative agreement with the experimental observations.

The shape of the stability chart is even more realistic in the third case we consider:

$$W(s) = \frac{1}{l}(1+\cos(\frac{\pi}{l}s))\,,\ s\in[-l,0]\,,\ \Rightarrow\ w(\theta) = \frac{1}{q\tau}(1+\cos(\frac{\pi}{q\tau}\theta))\,,\ \theta\in[-q\tau,0]\,. \tag{51}$$

If this weight function is substituted in (41) and (43), the functions

$$R_0(\psi) = (1-\cos\psi)\frac{\pi^2\sin(q\psi)}{q\psi(\pi^2-q^2\psi^2)} + \sin\psi\frac{\pi^2(1-\cos(q\psi))-2q^2\psi^2}{q\psi(\pi^2-q^2\psi^2)}\,,$$
$$S_0(\psi) = \sin\psi\frac{\pi^2\sin(q\psi)}{q\psi(\pi^2-q^2\psi^2)} - (1-\cos\psi)\frac{\pi^2(1-\cos(q\psi))-2q^2\psi^2}{q\psi(\pi^2-q^2\psi^2)}\,,$$

can be calculated and inserted into the calculation of the stability chart with (45) and (46). This is shown in Figure 11, where the improved stability properties can be detected both at low and high cutting speeds.

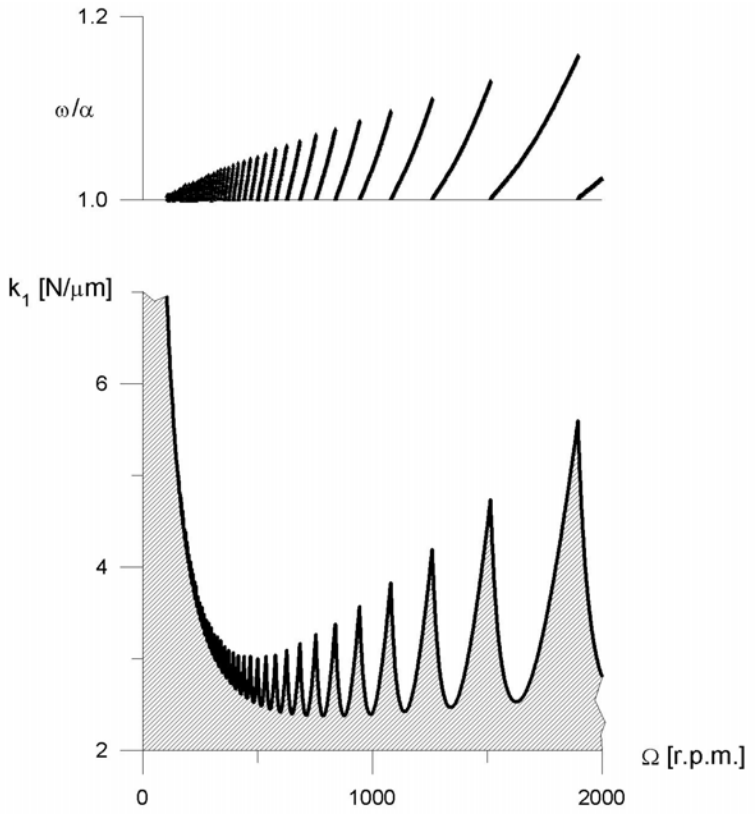

Figure 10: Stability chart with stress distribution (50), $q_0 = 0.01$

Finally, we present the stability chart for the weight function

$$W(s) = -\frac{\pi}{2l}\sin(\frac{\pi}{l}s)\,,\ s \in [-l, 0]\,, \quad \Rightarrow \quad w(\theta) = -\frac{\pi}{2q\tau}\sin(\frac{\pi}{q\tau}\theta)\,,\ \theta \in [-q\tau, 0]\,. \tag{52}$$

The corresponding stability chart is calculated using the functions

$$R_0(\psi) = \frac{\pi^2}{2}\left((1-\cos\psi)\frac{1+\cos(q\psi)}{\pi^2 - q^2\psi^2} + \sin\psi\frac{\sin(q\psi)}{\pi^2 - q^2\psi^2}\right)\,,$$
$$S_0(\psi) = \frac{\pi^2}{2}\left(\sin\psi\frac{1+\cos(q\psi)}{\pi^2 - q^2\psi^2} - (1-\cos\psi)\frac{\sin(q\psi)}{\pi^2 - q^2\psi^2}\right)$$

in the stability limits (45) and (46). The chart in Figure 12 is presented for low damping ($\kappa = 0.01$). It has a very complicated structure with a rich frequency content which may be very surprising from technical viewpoint. However, this chart may still describe a realistic situation: in case of

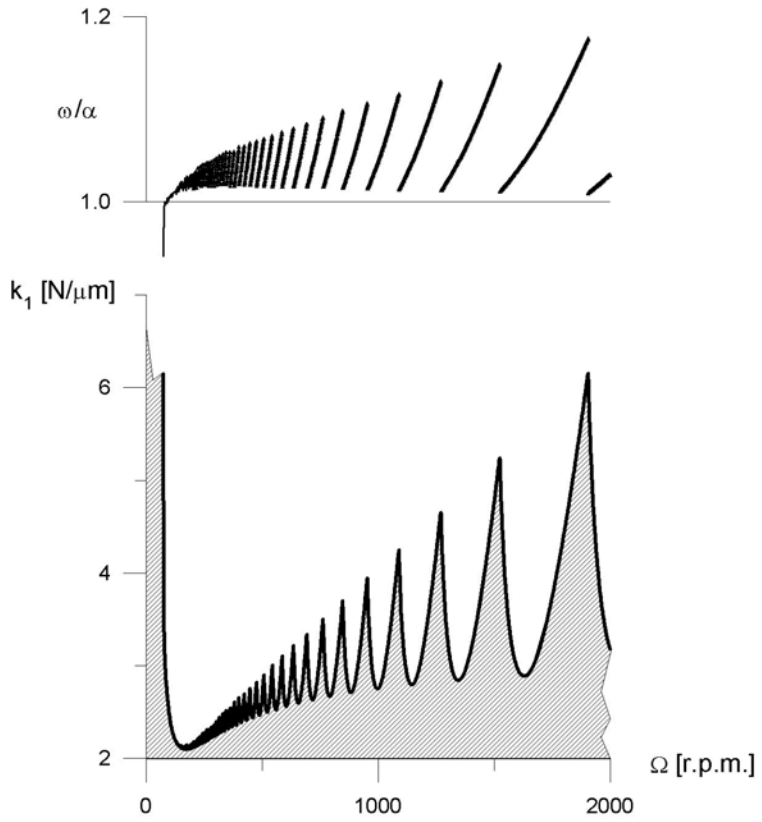

Figure 11: Stability chart with stress distribution (51), $q = 0.01$

drilling, the ratio of the short delay and the long one gets close to 1, and the maximum of the distributed cutting force is 'behind' the tool edge because of the negative rake angle at the chisel edge of the drill.

5 NON-LINEAR REGENERATIVE VIBRATIONS OF MACHINE TOOLS

The stability charts of cutting under regenerative conditions may refer to very complex linear stability properties depending on the technological and mechanical parameters, but the practical applicability of the results is still very limited. Apart of the uncertainty in the identification of some of the parameters, this is due to the fact that the domain of attractivity of the stable

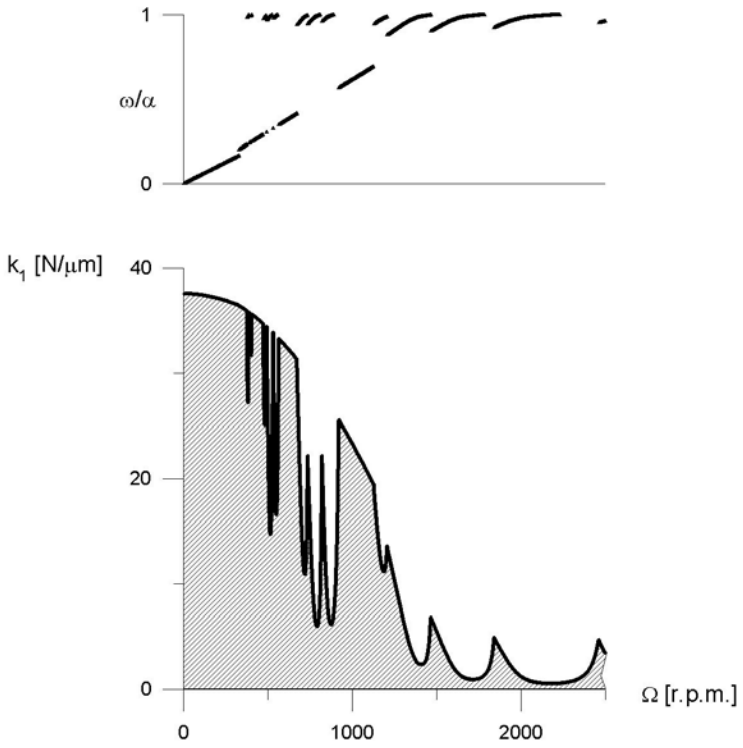

Figure 12: Stability chart with stress distribution (52), $q = 0.2$

stationary cutting may still be very small in the infinite dimensional phase space. In other words, relatively small perturbations may push the system away from the otherwise asymptotically stable equilibrium, and the arising non-linear vibrations will survive. This was clearly proved experimentally (Shi and Tobias 1984).

Two important reasons of non-linear regenerative vibrations are discussed qualitatively in this section. Both are related to the non-linearity of the cutting force shown in Figure 8, and also in the cutting force variation formula (34). First, consider the 'local' non-linearity of the cutting force, when it is assumed that the vibration amplitudes are still small in the sense that the tool does not leave the material of the workpiece:

$$x(t) < f_0 + x(t - \tau)\,.$$

The stability charts of Figures 9, 10, 11, 12 show that Hopf bifurcation occurs

at the stability limits, that is stable or unstable periodic motions exist around the equilibrium depending on the nature of the bifurcation, whether it is supercritical or subcritical, respectively. The approximate frequency of these vibrations is ω which is usually somewhat above the natural frequency of the system.

The algorithm of the Hopf bifurcation calculation has been worked out in the literature (Hassard, Kazarinoff and Wan 1981), and computer algebra may help carrying out the tedious algebraic calculations. A 3rd degree approximation of the cutting force at the desired chip thickness f_0 will contain also 2nd degree terms since the cutting force variation is not symmetric there. This makes the calculation even more difficult, since the center manifold, the critical invariant two-dimensional surface embedded in the infinite dimensional phase space, cannot be approximated by its tangent plane at the origin only, the determination of its 2nd degree approximation is also required. The result of this calculation is a closed form algebraic approximation of the periodic motion, and its stability is also determined. Note that co-dimension 2 bifurcations may also occur referring to the existence of stable or unstable quasiperiodic oscillations (tori) in the phase space with those frequencies where discontinuity appears in ω above the stability charts. Examples for such detailed calculations are presented in the literature (Stépán and Haller 1995; Campbell, Bélair, Ohira and Milton 1993) for robotics and population dynamics, respectively.

Some numerical examples show that the Hopf bifurcation in regenerative machine tool virations is subcritical, there is no evidence or mathematical proof that it cannot be supercritical in other cases, though. The experiments (Shi and Tobias 1984) also refer to the existence of unstable periodic motions. Figure 13 presents a simplified bifurcation diagram when the cutting force coefficient (or the width of cut) is the bifurcation parameter. The dashed curve refers to the unstable periodic motion or limit cycle, and this Hopf bifurcation calculation does not show any attractor around the unstable equilibrium (dashed line) or outside the unstable limit cycle.

There must be an attractor somewhere 'outside'. Consequently, the Hopf bifurcation cannot describe that attractor, and another, say 'global' non-

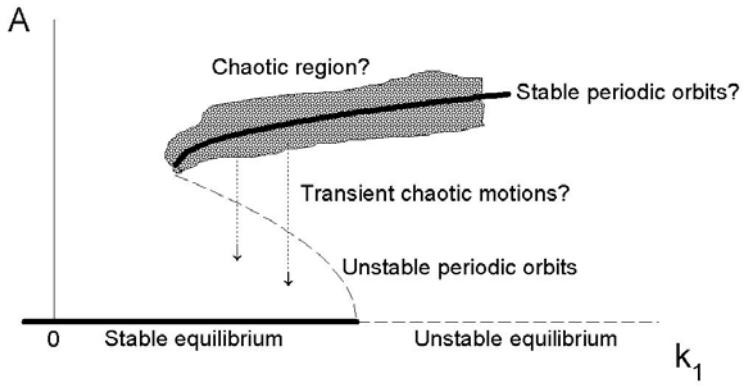

Figure 13: Bifurcation diagram

linearity must also be considered. This will be served by that part of the cutting force where the tool leaves the workpiece:

$$x(t) \geq f_0 + x(t-\tau)\,.$$

This is presented with respect to the cutting force variation in formula (34). For the time being, simulation seems to be the only way to get any information about the DDE model with this kind of nonlinearity. However, the existence of an attractor due to this global non-linearity can easily be explained qualitatively. If the system parameters are taken from the unstable region of the stability chart, or they are from the stable region but the perturbations are great enough to push the state variables outside the unstable periodic motion, then the coordinate x increases, and the tool sooner or later leaves the workpiece. At this point the cutting force becomes zero (or in other words, the cutting force variation in (34) becomes the constant $-F_x^T(f_0)$), and the regenerative effect is 'switched off'. This non-linearity is extremely strong: the delay effect in the infinite dimensional phase space is valid for a certain region of this phase space only, and the trajectories spiralling outwards will hit an (eventually also infinite dimensional) surface from where they jump onto the two dimensional phase plane of a simple oscillator, which refers to the motion of the free tool outside the workpiece material. That motion is damped, of course, and the tool will soon return to the workpiece.

There are several options then. The tool may arrive back from the phase plane into the infinite dimensional phase space outside the unstable limit cycle. Then it goes out again, and a series of switches occur between the two dynamics: the infinite dimensional delayed one, and the 2 dimensional dynamics of the simple oscillator. The result of these switches could either be some stable periodic or quasiperiodic motion, or a chaotic one. The observation of the fractal-like surfaces of the workpieces (Moon 1994) also confirm the possible existence of chaos in these systems. The third option is that transient chaotic motion occurs, since after some chaotic jumps between the two dynamics, the trajectory may arrive back to te delayed dynamics inside the unstable limit cycle, and the temporary chaotic motion of the system will settle at the stable stationary cutting. However, the length of this transient chaotic motion varies stochastically, and might be so long that the cutting process is already over. The structure of the transient chaotic motion here is the same as that of the shimmy problem of towed wheels (Stépán 1992) in a higher dimensional phase space, though.

6 CONCLUDING REMARKS

Regenerative vibrations are one of the most important reasons of machine tool vibrations. The delay-differential equation models of regenerative vibrations describe a very rich dynamics since the corresponding phase space is infinite dimensional. Even the linear stability analysis of these models serve an interesting and complex view of these systems and the stability charts in the space of the technological parameters may present fractal-like stability domains. Non-linear vibrations refer to the existence of unstable periodic motions, the co-existence of quasiperiodic and chaotic motions is also likely. Transient chaotic motions may also occur in some parameter domains. In the view of these DDE models we can conclude that the prediction of machine tool vibration is difficult even if we have a reliable mechanical and mathematical model at hand.

7 ACKNOWLEDGEMENTS

This research was partially supported by the Hungarian Scientific Research Foundation OTKA Grant No. 4-041, and the US-Hungarian Science and Technology Program Grant No. 336.

REFERENCES

Campbell, S. A., Bélair, J., Ohira, T., and Milton, J. (1995) *Journal of Dynamics and Differential Equations* 7 (1), 213-236.

Hale, J. K. (1977) *Theory of Functional Differential Equations*, Springer, New York.

Hassard, B. D., Kazarinoff, N. D., and Wan, Y. H. (1981) *Theory and Applications of Hopf Bifurcations*, London Mathematical Society Lecture Note Series 41, Cambridge.

Kuang, Y. (1993) *Delay Differential Equations*, Academic Press, Boston.

Marusich, T. D., and Ortiz, M. (1996) to appear in *Journal of Engineering Industry.*

Minis, I., and Yanushevsky, R. (1993) *Journal of Engineering Industry* 115 (2), 1-8.

Moon, F. C. (1994) in *Nonlinearity and Chaos in Engineering Dynamics* (Thompson, J. M. T., and Bishop, S. R., eds.), pp. 25-37, Wiley, Chichester.

Shi, H. M., and Tobias, S. A. (1984) *Int. J. of Machine Tool Design and Research* 24, 45-69.

Stépán, G. (1989) *Retarded Dynamical Systems*, Longman, Harlow.

Stépán, G. (1992) *Vehicle Systems Dynamics* 20, 341-351.

Stépán, G., and Haller, G. (1995) *Nonlinear Dynamics* 8, 513-528.

Tlusty, J., and Spacek, L. (1954) *Self-Excited Vibrations on Machine Tools* (in Czech), Nakl CSAV, Prague.

Tlusty, J. (1978) *Annals of the CIRP* 27 (2), 583-589.

Tobias, S. A. (1965) *Machine Tool Vibrations*, Blackie, London.

Usui, E., Shirakashi, T., and Kitagawag, T. (1978) *Journal of Engineering for Industry* 100 (5), 236-243.